ChemSusChem

Chemistry–Sustainability–Energy–Materials

Chemistry Europe

European Chemical Societies Publishing

Accepted Article

Title: Electrochemical conversion of CO2 to CO by a competent Fe(I) intermediate bearing a Schiff base ligand

Authors: Ruggero Bonetto, Roberto Altieri, Mirko Tagliapietra, Antonio Barbon, Marcella Bonchio, Marc Robert, and Andrea Sartorel

To be cited as: *ChemSusChem* 10.1002/cssc.202001143

Link to VoR: https://doi.org/10.1002/cssc.202001143

WILEY-VCH

WILEY-VCH

FULL PAPER

Electrochemical conversion of CO_2 to CO by a competent Fe(I) intermediate bearing a Schiff base ligand

Ruggero Bonetto,[a] Roberto Altieri,[a,b] Mirko Tagliapietra,[a] Antonio Barbon,[a] Marcella Bonchio,[a] Marc Robert[b,c]* and Andrea Sartorel[a]*

Abstract: Iron complexes with a N_2O_2 type, *N,N'-o*-phenylenebis(salicylimine) salophen ligand, catalyze the electrochemical reduction of CO_2 to CO in acetonitrile with phenol as the proton donor leading to 90 ÷ 99% selectivity, Faradaic efficiency up to 58%, and turnover frequency up to 10^3 s^{-1} at an overpotential of 0.65 V. This novel class of molecular catalyst for CO_2 reduction operate through a mononuclear Fe^I intermediate, with phenol being involved in the process with first order kinetics. The molecular nature of the catalyst and the low cost, easy synthesis and functionalization of the salophen ligand paves the way for catalyst engineering and optimization. Competitive electrodeposition of the coordination complex at the electrode surface results in the formation of iron based nanoparticles, which are active towards heterogeneous electrocatalytic processes mainly leading to proton reduction to hydrogen (Faradaic efficiency up to 80%), but also to the direct reduction of CO_2 to methane with a Faradaic efficiency of 1 ÷ 2 %.

Introduction

Activation of ubiquitous small molecules – i.e. chemically simple, naturally abundant and low molecular weight starting reagents – is a primary task with potential impact both in synthetic and energy-oriented strategies.[1],[2],[3] Two of the most targeted molecules are water and carbon dioxide: they represent the richest source of hydrogen and carbon in nature. In particular, the activation of carbon dioxide[4,5],[6],[7] and its subsequent conversion into useful chemicals upon reduction processes, is a primary goal of artificial photosynthesis, aiming at the production of renewable fuels by exploiting solar light. The reduction of CO_2 can proceed via 1 to 8 electrons, depending on the reaction products, and can be accomplished through the application of a negative potential to an electrode; in addition, the inertness of CO_2 calls for the use of catalytic routines to overcome the energy barriers associated to its reduction, with both heterogeneous[8–10],[11,12],[13] and homogeneous electrocatalysts[14],[15] being developed.

In the field of homogeneous molecular catalysis for CO_2 reduction, research has been intensively focused towards redox active coordination complexes of transition metals. Seminal works have been directed towards the use of second and third row transition metals,[3,16],[17,18] while recently considerable efforts have been directed to first row transition metals, with manganese, iron, cobalt, nickel, and copper being nowadays the preferred choice in the design and optimization of catalysts.[15],[19–21] The potential of molecular catalysis in this field has been recently shown in the application of a cobalt phthalocyanine[22] capable of mediating CO_2 to CO conversion with >95% selectivity in a flow cell operating at current density ≥ 150 mA cm^{-2},[23] and by embedding a cobalt porphyrin in a photoelectrochemical cell for syngas production, with solar–to–fuel efficiency in the range 0.02 ÷ 0.06%.[24]

A paramount role in the development of molecular catalysts for CO_2 reduction has been covered by iron complexes. Iron is the most abundant transition metal on Earth and its coordination chemistry is vast and may be bent to match several catalyst design requirements. Nature itself has developed iron-based enzymatic active sites which can evolve carbon monoxide from CO_2. The most notorious example is CO dehydrogenase, found in *Carboxydothermus hydrogenoformans* microorganism,[25,26] whose catalytic activity relies on the presence of a polynuclear metallic cluster, in which a [NiFe] CO_2 binding and activation site is coupled with an iron–sulfur cluster.[27] This system is highly efficient, reaching turnover frequency (TOF) higher than $3 \cdot 10^4$ s^{-1}. The development of efficient molecular CO_2 reduction catalysts displaying low operating overpotential (η), high kinetic constants and associated *TOF*, high turnover number (*TON*), Faradaic efficiency (*FE*) and chemical selectivity (see Table S1 in Supporting Information), is therefore intrinsically entailed with a biomimetic research focus. A related synthetic polynuclear iron complex was developed by Berben et al.,[28–30] and was proven as a versatile catalyst, whose selectivity may be driven towards formic acid or hydrogen generation by choosing the strength of the proton donor employed as co-catalyst, with stronger acids preferentially yielding H_2 with respect to HCOOH.

Besides this example, most of the iron based electrocatalysts for CO_2 reduction are based on single site complexes, with iron porphyrins standing as the current benchmark of reactivity (see Table S1, and the Catalytic Tafel plot graphical representation in Figure S1 in Supporting Information).[31,32] This family of catalysts is highly selective for CO_2–to–CO reduction with almost quantitative Faradaic efficiency, and operating through a Fe^0

[a] R. Bonetto, R. Altieri, M. Tagliapietra, Prof. A. Barbon, Prof. M. Bonchio, Prof. A. Sartorel
Department of Chemical Sciences
University of Padova
Via Marzolo, 1 35131 Padova, Italy
E-mail: andrea.sartorel@unipd.it
[b] Prof. M. Robert
Laboratoire d'Electrochimie Moléculaire
Université de Paris, Laboratoire d'Electrochimie Moléculaire, CNRS, F-75006 Paris, France
E-mail: robert@uparis.fr
[c] Prof. M. Robert
Institut Universitaire de France (IUF), F-75005 Paris, France.

Supporting information for this article is given via a link at the end of the document.

intermediate capable of CO_2 coordination and reduction.[33] Convenient functionalization of the porphyrin ring lead to a boost of the catalytic activity, by exploiting local proton sources[34] or supramolecular interactions with the CO_2 substrate.[35]

Recent work on iron catalysts focused on the use of complexes with *non–heme* polydentate nitrogen based ligands, such as the N_5–macrocyclic 2,13–dimethyl–3,6,9,12,18–pentaazabicyclo–[12.3.1]octadeca–1(18),2,12,14,16–pentaene,[36] and the 2,2′:6′,2″:6″,2‴-quaterpyridine (qpy).[37,38] In both cases, the proposed active species is a Fe^{I} intermediate, that leads to formic acid as the preferential product in the case of the complex with the N_5–macrocyclic ligand,[36] and to CO in the case of the Fe(qpy) species (see Table S1 in Supporting Information).[37,38] Iron complexes with tetradentate N_2O_2 ligand motifs have been less studied, with examples that exploit 2–hydroxybenzene pendants on 1,10–phenantroline or of 2,2'–bipyridine scaffolds.[39],[40] These species perform CO_2 reduction through a Fe^{I} intermediate obtaining mixtures of products, with formate being the dominant one.[39],[40]

The present work reports on iron complexes bearing an N_2O_2 type, salophen ligand L = *N,N′–o*–phenylenebis(salicylimine), as a novel class of homogeneous catalysts for CO_2 electrochemical reduction to CO, Scheme 1. Schiff base metal complexes represent structurally simple, and yet often effective, wide range molecular catalysts,[41–43],[44] and therefore offer an important and scalable alternative with respect to ligands that pose a severe synthetic challenge.

We show herein that: i) Fe–salophen undergo interconversion between mononuclear and dinuclear species through acid/base reactions, whereby mononuclear species are favoured in the presence of proton donors; ii) the electrochemical reduction of CO_2 to CO occurs in the presence of phenol as the proton donor through generation of a mononuclear Fe^{I} intermediate (Scheme 1, homogeneous route), with remarkable performance in terms of overpotential (η = 0.65 V) and rate (k_{cat} up to 10^3 s^{-1}); iii) the Fe^{I} intermediate undergoes competitive degradation through electrodeposition of Fe based nanoparticles at the carbon electrode, that are responsible for proton reduction to hydrogen, with a minor formation of methane (scheme 1, heterogeneous route).

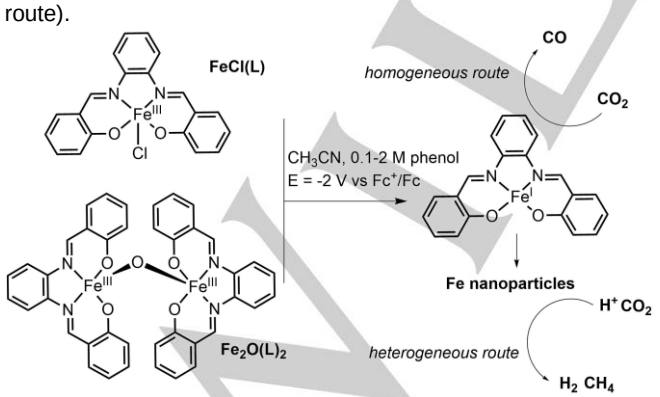

Scheme 1. Electrocatalytic reduction of CO_2 to CO (homogeneous route) by Fe-salophen complexes FeCl(L) and $Fe_2(\mu–O)(L)_2$ through a mononuclear Fe(I) intermediate, responsible also for electrodeposition of Fe nanoparticles that are active towards the hydrogen evolution reaction and methane formation (heterogeneous route).

Results and Discussion

Rationale. Salophen ligand is easily synthesizable from commercially available reagents; the idea of investigating its iron complexes for electrocatalytic reduction of CO_2 originated from previous observations in the literature. The electrochemical properties of FeCl(L) have been the subject of seminal research in the field of electrocatalysis by Bond and coworkers,[45] that identified sequential reduction of the Fe^{III} center to Fe^{II} and finally to Fe^{I}, with this latter species being electrocatalytically active towards reductive dehalogenation of benzyl halides.[45] Furthermore, the analog cobalt(II) salophen complex was reported as a CO_2–to–CO reduction electrocatalyst by Isse et al.,[46] involving an electrogenerated cobalt(I) active intermediate. Indeed, several examples in the literature showed a common, privileged ligand choice for the design of cobalt and iron CO_2 reduction catalysts.[29,30,31],[47],[48] This experimental Co/Fe analogy may originate from similar electronic features and operating potentials for reduced Fe and Co complexes; although it is still not fully elucidated from a mechanistic point of view, it can help in the design of new catalysts and lies at the basis of several investigation, including ours.

Synthesis and electrochemical features of mononuclear and dinuclear Fe complexes. Mononuclear FeCl(L) and μ-oxo dinuclear $Fe_2(\mu–O)(L)_2$ complexes were synthesized in 60 ÷ 65 % yield by a slight modification of literature procedures, that involve the addition of an iron precursor ($FeCl_3·6H_2O$ and $Fe(NO_3)_3·9H_2O$ for FeCl(L) and $Fe_2(\mu–O)(L)_2$, respectively) to a solution of the salophen ligand in ethanol, in the presence of triethylamine as base additive, followed by precipitation and washing of the product.[45,49] Distinctive features between FeCl(L) and $Fe_2(\mu–O)(L)_2$ can be evidenced through electrospray ionization mass spectrometry (ESI–MS) and UV/visible spectroscopy. In particular, ESI–MS spectra of both compounds exhibit an intense peak at m/z = 370, attributed to the $[Fe(L)]^+$ ion (Figure S2), while peaks attributed to dinuclear ions and centered at m/z = 757 ($[Fe_2(L)_2(\mu–OH)]^+$) and 785 were observed only in the case of $Fe_2O(L)_2$ (Figure S2). Concerning UV/Vis spectroscopy, the two coordination compounds exhibit a notably different electronic absorption (Figure S3), consistent with literature references.[45,49] A band peaking at 365 nm ($\varepsilon = 1.3·10^4$ M^{-1} cm^{-1}) is observed for FeCl(L), while the dinuclear $Fe_2(\mu–O)(L)_2$ complex is characterized by a redshifted maximum at 405 nm ($\varepsilon = 2.0·10^4$ M^{-1} cm^{-1}); these spectral features, absent for the free ligand and characterized by high intensity and molar extinction coefficients, could therefore be appropriately described as charge-transfer bands between the Fe ions and the salophen ligand.

A different behaviour between FeCl(L) and $Fe_2(\mu–O)(L)_2$ is also observed in cyclic voltammetry. The CV trace of the mononuclear FeCl(L) (0.8 mM in acetonitrile with 0.1 M tetrabutylammonium tetrafluoroborate, Figure 1) displayed a first reversible cathodic process at $E_{1/2}$ = – 0.69 V vs Fc^+/Fc (ΔE = 84 mV) attributed to the Fe^{III}/Fe^{II} couple, followed by a second, quasi-reversible one at $E_{1/2}$ = – 2.00 V vs Fc^+/Fc, and attributed to reduction of Fe^{II} to Fe^{I}.[45] For $Fe_2(\mu–O)(L)_2$ the first, quasi-reversible cathodic wave encountered in the forward scan is cathodically shifted ($E_{1/2}$ = – 1.32 V vs Fc^+/Fc, ΔE = 100 mV) and is attributed to the Fe^{III} to

Fe^{II} reduction of both iron centers of the Fe–O–Fe μ-oxo bridge.[49] The more negative potential required to reduce Fe^{III} to Fe^{II} in the dinuclear species with respect to the mononuclear one is in agreement with previous literature,[49] and was observed also for iron porphyrin analogs.[50] This is likely attributed to injection of electrons into high energy π* orbitals delocalized on the three FeOFe atoms in the dinuclear species.[51] In addition, the non–reversibility of the wave was attributed to partial dissociation of the dinuclear species into two mononuclear units behaving independently.[49] This was further confirmed by the two anodic peaks observed in the backward scan, at anodic peak potential E_{pa} = – 1.28 V vs Fc^+/Fc (re–oxidation of Fe^{II} to Fe^{III} in the dinuclear species) and at E_{pa} = – 0.65 V vs Fc^+/Fc, attributable to the re–oxidation of Fe^{II} to Fe^{III} in a mononuclear unit. Regarding this last aspect, a similar behaviour was also observed for porphyrin analogs.[50]

Scanning toward more negative potentials with $Fe_2(\mu–O)(L)_2$, a quasi-reversible wave at $E_{1/2}$ = – 2.00 V vs Fc^+/Fc was observed and attributed to the expected reduction of Fe^{II} to Fe^{I} in a mononuclear species.[49] The formation of a common, mononuclear Fe^{I} species either starting from FeCl(L) or from $Fe_2(\mu\text{-}O)(L)_2$ was further confirmed by spectro-electrochemistry in the UV-Vis region, that shows an identical absorption centered at 405 nm upon application of – 2.00 V vs Fc^+/Fc potential for both complexes (Figure S4). The redshift with respect to the pristine Fe^{III} species is consistent with an iron–to–ligand charge transfer band from a reduced iron center.[51]

Interconversion of mononuclear and dinuclear species. The distinctive spectral and electrochemical features of the mononuclear and dinuclear salophen–based Fe species allow their speciation in solution, and the investigation of their interconversion in the presence of Brønsted acids or bases additives. From literature evidence and from chemical considerations regarding the nature of the complexes, the μ–oxo bridge binding the two Fe centers in the $Fe_2(\mu–O)(L)_2$ should form between two mononuclear units, in a base-induced condensation reaction; indeed, conversion of FeCl(L) into $Fe_2(\mu–O)(L)_2$ upon addition of NaOH was observed through cyclic voltammetry, that revealed the progressive abatement of the Fe^{III}/Fe^{II} diagnostic peak for FeCl(L) ($E_{1/2}$ = – 0.69 V vs Fc^+/Fc), accompanied by a rise of the cathodic peak related to the dinuclear $Fe_2(\mu–O)(L)_2$ ($E_{1/2}$ = – 1.28 V vs Fc^+/Fc), Figure 1 (consistently, a progressive modification of the UV/Vis spectra was observed, see Figure S3).[52]

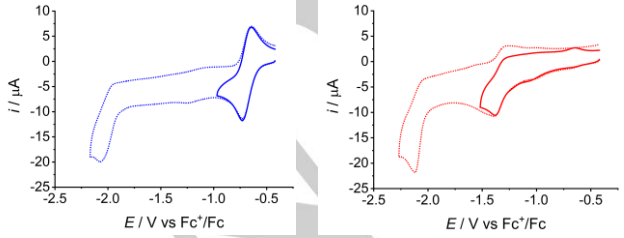

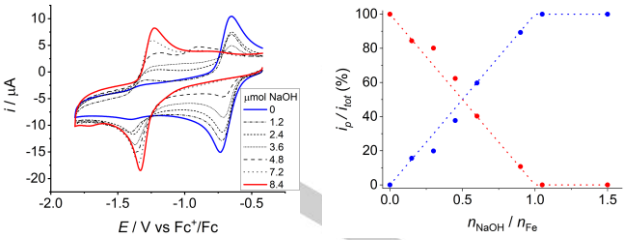

Figure 1. Cyclic voltammetry of 0.8 mM FeCl(L) (top left) and of 0.4 mM $Fe_2(\mu–O)(L)_2$ (top right) in nitrogen saturated CH_3CN with 0.1 M $TBABF_4$. Bottom left: cyclic voltammetry of 0.8 mM FeCl(L) upon progressive addition of NaOH; it is worth to highlight that in these CV the wave at – 1.25 V attributed to the dinuclear species has a higher degree of reversibility with respect to the one registered for the $Fe_2(\mu–O)(L)_2$ (see top right panel); the reversibility of the process was indeed shown to depend on the presence of electrolytes.[49] Bottom right: plot of the i_p/i_{tot} observed in Fe(L)Cl titration, versus the equivalents of NaOH added with respect to the iron centers. Blue dots: i_p measured at a peak potential E_p in the range – 0.74 to – 0.71 V, associated to FeCl(L); red dots: i_p measured at E_p = – 1.40 V to – 1.33 V, associated to $Fe_2(\mu–O)(L)_2$. Potentials are reported versus Fc^+/Fc, scan rate 0.1 Vs^{-1}. The dotted traces are added for visualization purposes and do not come from fitting.

On the opposite site, protolysis of the μ–O bridge[53,54] in the presence of Brønsted acids leads to the formation of mononuclear units $Fe(L)^+$ from $Fe_2(\mu–O)(L)_2$ (see Figure S5 in Supporting Information showing the $Fe_2(\mu–O)(L)_2$ conversion to $Fe(L)^+$ in the presence of acetic acid); the $Fe(L)^+$ may lead to the formation of FeCl(L) in the presence of chloride ions (Scheme 2 and Figure S5). The reversible interconversion between mononuclear and dinuclear species can be summarized in Scheme 2; in particular, the conversion of dinuclear into mononuclear species in the presence of proton donors is of particular relevance, since the presence of a proton source is typically needed in investigating the electrocatalysis of CO_2 reduction; the intrinsic instability of the μ–oxo bridge under the conditions for electrochemical CO_2 reduction hampers an evaluation of the impact of the nuclearity of the iron complex on the reactivity in the present case (*vide infra*).

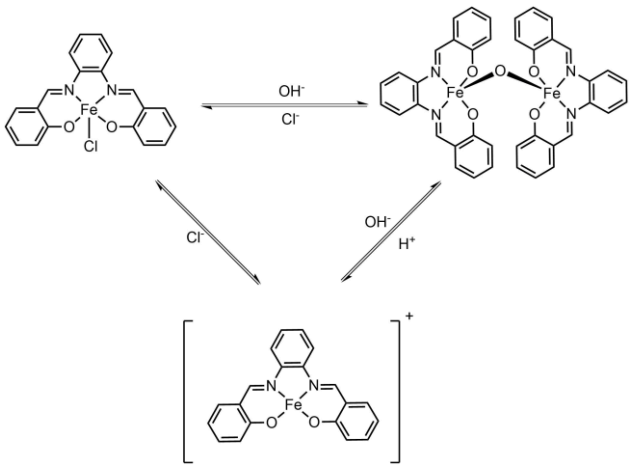

Scheme 2. Equilibria among mononuclear and dinuclear iron complexes with salophen ligand. Further apical ligands of iron centers are omitted for clarity.

Electrochemical behavior of salophen-based Fe in the presence of carbon dioxide. The voltammogram of CO_2–saturated solutions of mononuclear FeCl(L) is reported in Figure 2 (see Figure S6 for the CV of $Fe_2(\mu–O)(L)_2$). For what concerns the Fe^{III}/Fe^{II} couple, no significant changes are observed; the Fe^{II}/Fe^{I} reduction peak, however, is affected by the presence of carbon dioxide, observing a two– to three– fold enhancement of the cathodic peak current (Figure 2 and Table 1). The registered increase of the peak current might be regarded as an electrocatalytic current contribution, as previously reported for the analogous Co^{II} complex,[46] where the increase of cathodic current under similar conditions was attributed to the electrochemical reduction of CO_2 to CO with formation of carbonate. Incidentally, the irreversible Fe^{II}/Fe^{I} peak shape, potential and current are similar for both mononuclear and dinuclear Fe catalysts, thus suggesting the occurrence of a redox process involving a common mononuclear Fe(I) intermediate (compare the traces of $Fe_2(\mu–O)(L)_2$ in Figure S6). A further confirmation came from similar traces observed under spectroelectrochemistry in the infrared region (SEC-IR), a widely utilized tool for characterizing binding and reduction of CO_2 at metal centers.[38,55],[39,40],[56]

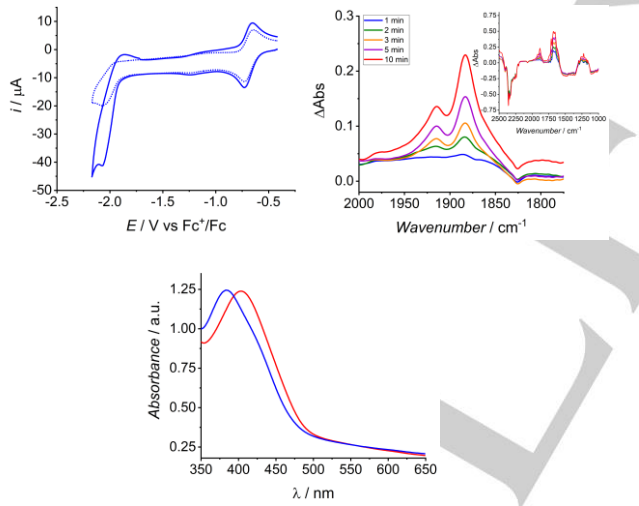

Figure 2. Left: cyclic voltammetry of 0.8 mM FeCl(L) under nitrogen saturated solution (pale colored trace) or under carbon dioxide saturated solution (deep colored trace). General conditions: CH_3CN with 0.1 M [TEA][BF_4]. Working electrode: glassy carbon; counter electrode: gold; reference electrode: Ag/AgCl, potentials are then converted versus Fc^+/Fc; scan rate: 0.1 Vs^{-1}. After the catalytic process, the raising of a new wave is observed at E ca –2.15 V, and is attributable to demetalation of the iron complexes (*vide infra*). Right: SEC–IR analysis conducted for FeCl(L) (0.8 mM) in the presence of CO_2. General conditions: CH_3CN with 0.1 M [TEA][BF_4]. Working electrode: Pt gauze; counter electrode: Pt; pseudoreference electrode: Ag wire, potentials are then converted versus Fc^+/Fc; applied potential E = – 2.1 V vs Fc^+/Fc. Bottom: SEC–UV/Vis analysis conducted for FeCl(L) (0.8 mM) at in the absence (red trace) and in the presence of CO_2 (blue trace). General conditions: CH_3CN with 0.1 M [TEA][BF_4]. Working electrode: Pt gauze; counter electrode: Pt; pseudoreference electrode: Ag wire, potentials are then converted versus Fc^+/Fc; applied potential E = – 2.1 V vs Fc^+/Fc.

The differential IR spectra obtained for FeCl(L) along SEC-IR experiments in the presence of CO_2, conducted at the potential of the second reduction, are reported in Figure 2 (SEC-IR of $Fe_2(\mu–O)(L)_2$ is reported in Figure S6). The low frequency, intense positive absorptions bands at 1883 cm^{-1} and 1913 cm^{-1} are reasonably attributed to the C–O stretching in an iron–carbonyl intermediate,[38],[39],[40] originated from iron assisted C–O bond breaking of carbon dioxide. Consistently, oxide transfer to a second molecule of CO_2,[46] in the presence of traces of water in the SEC cell, leads to hydrogen carbonate[57,58] as supported by the positive absorptions bands at 1679, 1646 and 1306 cm^{-1} (inset in Figure 2 bottom). Finally, the negative absorptions at 2357 and 2324 cm^{-1} are ascribed to CO_2 consumption along the electrolysis (inset in Figure 2, bottom).[39] A further evidence of Fe^{I} reactivity towards CO_2 comes from spectroelectrochemistry in the UV/Vis (SEC–UV/Vis), where the maximum of absorption of Fe^{I} at 405 nm shifts to 385 nm in the presence of CO_2, which can be ascribed to the formation of the same iron carbonyl intermediate detected by SEC–IR (Figure 2; see Figure S6 for analogous experiment conducted on the dinuclear species).

The formation of an iron carbonyl intermediate implies a prior binding of CO_2 to the iron center; a preliminary attempt to characterize such key intermediate was performed by generating the Fe^{I} species by bulk electrolysis, followed by bubbling of CO_2 in the absence of applied potential (therefore under different conditions with respect to the SEC analysis). The UV/Vis analysis of the Fe^{I} shows a marked change after bubbling of CO_2, with a blue shift of the maximum from 405 nm to 370 nm, together with an increase of absorption intensity below 400 nm, while an abatement of absorption intensity above 500 nm occurs (Figure S7 in Supporting Information). This spectrum is different with respect to the one of the Fe–carbonyl observed under SEC-UV/Vis (Figure 2 bottom) while showing instead similar features with respect to the one of Fe^{III} (Figure S7). This result suggests the reactivity of Fe^{I} intermediate towards CO_2, associated to the oxidation of the iron center. A further evidence of reactivity and oxidation of Fe^{I} in the presence of CO_2 came from electron paramagnetic resonance (EPR) spectroscopy. For a frozen sample of the electrogenerated Fe^{I} state, a signal at 3450 G ($g \approx 2$) is observed at 80 K, which is consistent with a S = ½ for a d^7 low–spin Fe^{I},[59] (Figure S8); in the sample treated with CO_2, the signal above disappears, while the appearance of a broad band at ca 3330 G and the raising of a feature at 1600 G ($g \approx 4.3$) were observed (Figure S8). These features are consistent with a d^5 high–spin Fe^{III} with a high degree of rhombicity,[60,61] formed upon reaction of Fe^{I} with CO_2. Interestingly, although indicative of a Fe^{III} state, this spectrum is different from the one of $Fe^{III}Cl(L)$, that shows a signal at low fields at g = 8.6 indicative of a smaller degree of rhombicity, likely ascribable to different apical ligands (Figure S8).

The enhancement of the current in the CV traces, associated with the generation of the electroactive iron(I) species in the presence of CO_2 is however modest. By assuming a reductive catalytic

process in which carbon dioxide is involved, the observation may be related to the absence of a catalyst coadjutant, in particular of a suitable proton donor.[33]

The chemical and electrochemical properties of the iron salophen species were thus investigated in the presence of Brønsted acids such as phenol (PhOH), acetic acid (HAc), and water.

In particular, phenol provided the most interesting results, based on its effectiveness as CO_2 reduction activity enhancer, already used in several literature examples of iron-based molecular catalysts (see Figure S9 for results with acetic acid and water).[33,62,63] This particular "CO_2 oriented selectivity" of phenol with respect to other proton donors may be related to its mild acidity (pK_a = 29.14 in acetonitrile[35]), that hampers the formation of iron hydride intermediates and their subsequent reaction with protons to form hydrogen.

Phenol was employed in excess (0.1 ÷ 2 M) with respect to the Fe species, as in previous relevant literature works; cyclic voltammetry traces of FeCl(L) are reported in Figure 3; the ones referring to $Fe_2(\mu\text{–}O)(L)_2$ are reported in Figure S10, where comparable results were obtained, since the presence of phenol induces protolysis and cleavage of the Fe–O–Fe μ–oxo group, leading to the generation of the mononuclear $Fe(L)^+$ (Scheme 2 and previous discussion).

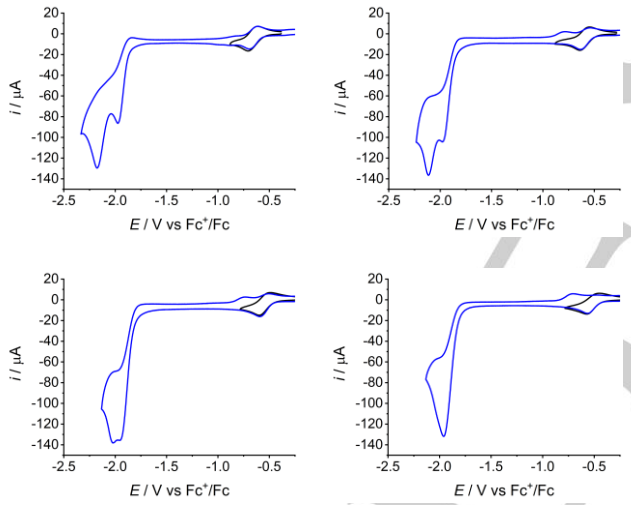

Figure 3. CV of 0.8 mM FeCl(L) under CO_2 saturated solutions, with different concentrations of phenol: 0.1 M (top left), 0.5 M (top right), 1 M (bottom left), 2 M (bottom right). General conditions: CH_3CN with 0.1 M $TEABF_4$, working electrode: glassy carbon; counter electrode: gold; reference electrode: Ag/AgCl, potentials are then converted vs Fc^+/Fc; scan rate: 0.1 V s^{-1}. See Figure S11 in Supporting Information for traces obtained with 0.2, 0.3 and 0.6 M phenol, and Figure S12 in Supporting Information for traces obtained under N_2 saturated solutions.

The results can be summarized as follows:

(i) in the presence of increasing concentration of phenol, the E^0_{app} of the Fe^{III}/Fe^{II} couple progressively shifts to less negative values (E^0_{app} values in the range between – 0.66 V and – 0.51 V vs Fc^+/Fc, Figure 3 and Figures S10 – S12), indicative of a preferential binding of phenol to Fe^{II} center. The anodic shift of the potential can indeed be fitted according to equation (1), see Figure S13 and discussion in Supporting Information:[38],[64]

$$E^0_{app} = E_{1/2} + RT/nF \cdot \ln\{1 + \beta_2[\mathrm{PhOH}]^2\} \qquad (1)$$

where β_2 is the formation constant of Fe^{II} salophen adduct with two phenol moieties (n = 1 in the Fe^{III}/Fe^{II} couple); fitting of the traces provides $\beta_2 = 170 \pm 11$ M^{-2} (Figures S11 – S13).

(ii) When the forward cathodic scan proceeds towards more negative potentials, the re–oxidation wave of the Fe^{III}/Fe^{II} couple splits into two components, where the one observed at more negative potentials (ca – 0.75 V vs Fc^+/Fc) is attributed to the Fe^{III}/Fe^{II} couple of the mononuclear iron complex $Fe(L)^+$ where the chloride ligand is displaced (see the CV of $Fe(L)^+$ in Figure S10 and S14 in Supporting Information; similar results are indeed obtained in the CV under N_2 atmosphere, Figure S12, with the concentration of phenol that impacts on the Cl^- displacement, as suggested by the increase of intensity of the wave at – 0.75 V vs the amount of phenol). [49],[65]

(iii) The scan towards more negative potentials is accompanied by the raising of the expected, intense and irreversible wave attributed to CO_2 reduction, at the potential of the Fe^{II}/Fe^{I} couple. The peak potential E_{p,CO_2} is observed at – 1.99 V, independently from phenol concentration, while the peak current i_{p,CO_2} raises from – 86 to – 136 μA (corresponding to – 1.22 to – 1.92 mA·cm^{-2}) upon increase of [PhOH], Figure 3. A visual analysis of the voltammogram reveals a peak–shaped wave,[31,55] suggesting the interference of secondary phenomena competing with catalysis (*vide infra*; increase of the scan rate up to 10 V s^{-1} did not change the current profile to an "S–shaped" wave, see Figure S15 in Supporting Information). Still, superimposable waves were observed in the voltammograms under CO_2 of $Fe(L)^+$ species deriving from $Fe_2(\mu\text{–}O)(L)_2$ at the same nominal iron concentration (0.8 mM, Figure S10).

(iv) The catalytic wave of CO_2 reduction is followed by a further intense wave, characterized by a peak current of ca – 130 μA and by a peak potential that depends on phenol concentration and falls in the range – 2.17 ÷ – 2.00 V vs Fc^+/Fc, with less negative values observed at high concentration of phenol. At the highest phenol concentrations employed (1 and 2 M), this wave partially superimposes with the catalytic wave of CO_2 reduction (Figure 3). Similar waves are observed also in the CV under N_2 (Figure S12 in Supporting Information) and are attributed to catalyst demetalation and electrodeposition[65] (further evidence will be provided by electrolysis experiments, *vide infra*).

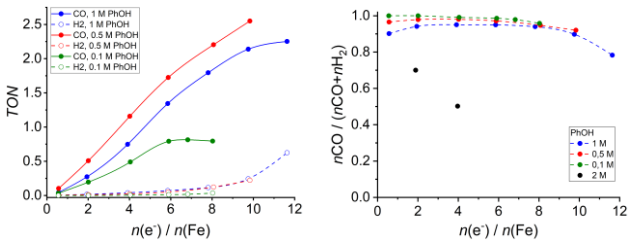

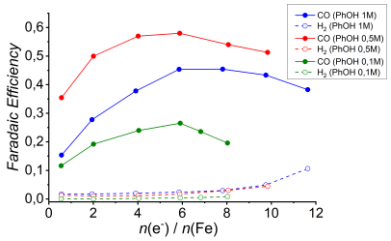

Figure 4. Turnover number for CO and H_2 (top left), selectivity for CO (top right) and Faradaic efficiency versus the charge passed along electrolysis experiments, normalized per Iron center, as a function of phenol concentration (0.1 ÷ 1 M; regarding selectivity, two data points for the electrolysis at 2 M phenol are also shown). General conditions: CH_3CN + 0.1 M $TEABF_4$, 2 M phenol, CO_2 saturated solution, FeCl(L) 0.8 mM. Working electrode: 2 cm^2 glassy carbon plate; counter electrode: platinum wire; reference electrode: Ag/AgCl, potential is then referred to the Fc^+/Fc couple for uniformity with other electrochemical data discussed in the manuscript; Electrolysis potential = – 2.0 V vs Fc^+/Fc. Lower *TON*, CO vs H_2 selectivity and *FE* were obtained in the presence of H_2O and HAc as proton donor (Figure S18).

In order to characterize the electrochemical processes associated with these cathodic waves, controlled potential electrolysis experiments (CPE) were conducted by employing a 2 cm^2 glassy carbon working electrode (see Figure S16 for total charge vs time profiles). Concerning the reaction products, both CO and H_2 were detected along the electrolysis, while no formic acid, methanol and other soluble products were observed. A control experiment employing $^{13}CO_2$ led to the formation of ^{13}CO, thus confirming carbon dioxide as the source of the produced carbon monoxide (Figure S17).

Interestingly, the formation of CO and H_2 showed markedly different profiles along the electrolysis, as can be appreciated in Figure 4, reporting the turnover number of FeCl(L) for CO and H_2 (top left), the selectivity for CO (top right) and the Faradaic efficiency (bottom) as a function of the charge passed during electrolysis, normalized per iron center (see also Table S2 in Supporting Information). In particular, employing PhOH in the range 0.1 ÷ 1 M, CO was detected from the beginning of the electrolysis with selectivity in the range 90 ÷ 99% and Faradaic efficiency up to 59%, while its production suffers from a slowing down after ca 10 electrons passed per iron center. Conversely, in all cases the H_2 profile showed an initial lag time followed by a rising of production, concomitant to the depletion of CO formation (total *TON* for CO production of 3, with 0.5 M [PhOH]) that leads to a drop of selectivity of the process after ca 10 electrons passed per Iron center in electrolysis (Figure 4; lower TON, CO vs H_2 selectivity and FE were obtained in the presence of H_2O and HAc as proton donor, see Figure S18).

The UV/Vis analysis of the electrolysis solution shows the fingerprint signatures of mononuclear $Fe(L)^+$ with a ca 20% abatement of intensity with respect to a freshly prepared solution at the same nominal concentration (Figure S19), indicating partial catalyst decomposition. Reutilization of this solution in a new electrolysis, after polishing of the working electrode, restores the production of CO; this result speaks in favour of a surface modification of the glassy carbon working electrode, originated from the decomposition of the iron catalyst, as responsible for the observed change of selectivity of the process towards hydrogen evolution. The change of catalytic regime was even more pronounced at a higher phenol concentration of 2 M, where a lower initial CO selectivity and its faster drop were observed (Figure 4).

Indeed, after the electrolysis experiment the glassy carbon working electrode surface was found to be covered by iron based nanoparticles originated from electrodeposition of the iron molecular precursor at the electrode, with rough surface and dimensions up to 100 nm, as revealed by Scanning Electron Microscopy (SEM, Figure S20 in Supporting Information). *Ex-situ* X-Ray Photoemission Spectroscopy (XPS) showed peaks at binding energies of 726 and 711 eV associated to Fe $2p_{3/2}$ and Fe $2p_{1/2}$ transitions, typical of iron oxide formed upon air exposure of the electrode (Figure S20 in Supporting Information).[67] The electrodeposition of the nanoparticles could likely originate from ligand demetalation upon a further reduction of Fe^I to Fe^0 intermediates, as observed in the case of the Fe(qpy) catalyst.[38,67] The direct utilization of the unpolished glassy carbon electrode in a CPE experiment, conducted in the absence of Fe complexes in solution, led to immediate, continuous and stable production of H_2 (current density = 0.6 mA·cm^{-2}, Faradaic efficiency in the range 65 ÷ 80%), while no CO was detected. Interestingly, methane was also observed as electrolysis product,[67] and confirmed to be electrogenerated from carbon dioxide from a labelling experiment with $^{13}CO_2$ (Figure S21), with a Faradaic efficiency of 1 ÷ 2 %; this value corresponds to a partial current density for methane generation in the range 6 ÷ 12 μA·cm^{-2}, slightly inferior to the one obtained in the case of Fe nanoparticles electrodeposited from Fe(qpy), 27 μA·cm^{-2}.[67] The yield and selectivity of methane generation likely depend on nanoparticles size, shape and composition.[67]

Homogeneous vs heterogeneous electrocatalytic routes and benchmarking. The results above can thus be interpreted on the basis of competitive homogeneous and heterogeneous electrocatalytic pathways having different preferential products. The former is carried out by the molecular Fe^I salophen intermediate, and leads to selective CO_2 reduction to CO (see proposed pathway in Scheme 3). The latter is driven by the heterogeneous iron nanoparticles formed upon electrodeposition from the molecular precursor,[67] and is mainly oriented towards proton reduction to H_2 with formation of CH_4 as a minor product (Scheme 1).

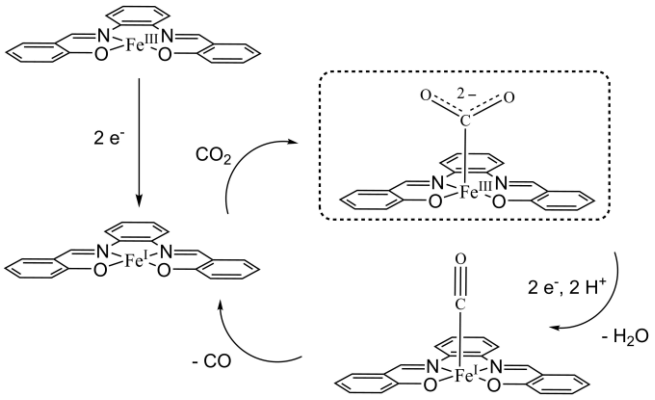

Scheme 3. Proposed mechanistic route towards molecular CO_2 reduction to CO through a Fe(I) intermediate. The exact sequence of electron and proton transfer from the Iron–CO_2 adduct to the Iron–carbonyl species is not known at the present stage. The oxidation states in the Iron–CO_2 intermediate are postulated on the basis of the EPR analysis discussed above.

From investigation of the homogeneous pathway leading to CO production, the catalytic current of CO_2 reduction to CO occurs at the level of the Fe^{I} intermediate. Iron porphyrins, the most investigated and active electrocatalysts for CO_2 reduction to CO, are known to operate through a Fe^{0} intermediate. Reported examples of complexes being active through a Fe^{I} intermediate deal with iron species with a N_5–macrocycle ligand[36] and with N_2O_2 ligands[39],[40] that are selective for formic acid, and of an iron complex with a qpy ligand[37,38] that shows selectivity towards CO. A favoured selectivity for CO with respect to HCOOH is typically determined by a preferred pathway of C–O bond breaking in a metal-CO_2 adduct, and requires a suitable balance of electron density at the metal center: excessive density at the metal may induce π-back-donation to π^* orbitals of CO_2, increasing the basicity of carbon and favouring formate type intermediates.[7] This was recently shown by Costentin and Nocera,[68] where selectivity of CO_2 reduction by Iron tetraphenylporphyrin was switched from CO to HCOOH in the presence of tertiary amines, acting as Lewis bases to the Iron center. Production of formic acid can occur also through reaction of CO_2 with a metal hydride intermediate, with sufficient hydricity.[36],[69]

With the identification of CO as the product of the homogeneous electrocatalytic reduction of CO_2 by Fe salophen species, it is possible to determine the metrics for catalyst benchmarking. The overpotential η can be calculated from the difference between the peak potential $E_{p,CO2}$ of the catalytic curve previously determined (Table 1) and the E^0 for the CO_2/CO couple under the adopted conditions. In organic solvents E^0 (CO_2/CO) is related to the following equation, and depends on the activity of the species including the acidity of the proton donor HA:

$$CO_2 + 2\,HA + 2\,e^- = CO + H_2O + 2\,A^-$$

This was recently estimated in acetonitrile as – 0.72 V *vs* standard hydrogen electrode (SHE),[62] resulting in E^0 (CO_2/CO) = – 1.34 V vs Fc^+/Fc after converting the potential to the Fc^+/Fc couple (E vs SHE = E vs Fc^+/Fc + 0.624 V).[70] Therefore, the overpotential at the peak of the wave in the presence of phenol can be calculated as:

$$\eta = -\,(E_{p,CO_2} - E^0(CO_2/CO)) = 1.99 - 1.34\ V = 0.65\ V$$

The k_{cat} of the iron complex at different phenol concentrations (in the range 0.1 ÷ 0.6 M, where the wave of CO_2 reduction is clearly distinguished from the wave of electrodeposition, see previous Figure 3), can be estimated from the foot-of-the-wave analysis (FOWA) of the voltammograms (Figure S22 in Supporting Information. FOWA can be used in molecular electrochemical catalysis, in particular when side phenomena (including substrate consumption) prevents from obtaining ideal "S-shaped" catalytic waves independent of scan rate, characteristic of pure kinetic conditions.[31,32] FOWA enables determination of the rate constant by analysis and fitting (according to the theoretical i = f(E) equation) of a CV scan at the foot of the catalytic wave, where low charge has passed and side phenomena can be assumed negligible.[31,32]

The plots show profiles with a maximum, as expected for the presence of side phenomena; the linear fitting are applicable only in a restricted range of low ($E - E^0_{Fe(II/I)}$) values, providing slopes that can be associated to the k through Eq. (2), where the concentration of CO_2 substrate is equal to 0.28 M in acetonitrile (see Figure S22 in Supporting Information):[35]

$$\text{slope} = 2.24\sqrt{2k\,x\,[CO_2]} \qquad (2)$$

The catalytic constants k_{cat} (Table 1) can then be calculated from Eq. (3):

$$k_{cat} = k \cdot [CO_2] \qquad (3)$$

The k_{cat} values show a linear dependence on phenol concentration, while the plot of $\log(k_{cat}/k_{cat0})$ vs $\log([PhOH]/[PhOH]_0)$ shows a slope of 0.82 (Figure S23 in Supporting Information), suggesting a first order dependence in the catalytic cycle of CO_2 reduction to CO. A catalytic scheme can thus be postulated, involving a $2e^-$ / $2H^+$ reduction of a Fe–CO_2 adduct, releasing CO and water, and regenerating the Fe^{I} resting state. It is worth to mention that the initial catalyst activation (reduction of Fe^{III} to Fe^{I} active state) can also account for the low Faradaic efficiency observed at the initial stage of the electrolysis ($n(e^-)/n(Fe)$ < 4, see Figure 4).

Table 1. Electrocatalytic parameters for reduction of CO_2 to CO by FeCl(L) determined from CV experiments. An uncertainty of ±5% should be considered for the i_p and k_{cat} values reported.

[PhOH], M	E_{p,CO_2},[a] V vs Fc^+/Fc	i_p,[a] µA (j_p, mA·cm^{-2})	k_{cat},[b] s^{-1}
–	– 2.07	– 41 (– 0.58)	0.60±0.03
0.1	– 1.99	– 86 (– 1.22)	291±15
0.2	– 1.99	– 91 (– 1.29)	421±20

0.3	– 1.99	– 98 (– 1.39)	531±26
0.5	– 1.99	– 100 (– 1.41)	1016±50
0.6	– 1.99	– 108 (– 1.53)	1250±60
1	– 1.99	– 136 (– 1.92)	n.d.
2	– 1.99	– 132 (– 1.87)	n.d.

[a] Determined from CV traces, see Figures 3 and S10. [b] Determined from the FOWA analysis, see Figure S21.

After determination of η and of k_{cat}, the values obtained at [PhOH] = 0.6 M were plotted as a catalytic Tafel plot (equation 4 and Figure 5). It summarizes the intrinsic performance of the catalyst upon correlating the turnover frequency *TOF* to the overpotential η under the assumption of fast electron transfer from the electrode to the catalyst, eq. (4) with $\eta = E^0_{CO_2/CO} - E$,[33] and allows for benchmark comparison with literature data (Figure S1 in Supporting Information).

$$TOF = \frac{k_{cat}}{1 + exp\left[-\frac{F}{RT}\left(E^0_{cat} - E^0_{CO2/CO}\right)\right] exp\left[-\frac{F}{RT}\left(E^0_{CO2/CO} - E\right)\right]}$$

(4)

In the left part of the graph, log(*TOF*) increases linearly with the overpotential η because the fraction of active catalyst in the reaction layer grows exponentially with η. The plateau on the right part of the graph log(TOF_{max}) is reached when the potential is negative enough to transform all the catalyst is in its active form (an ideal catalyst should display a minimum overpotential and a large TOF_{max}).

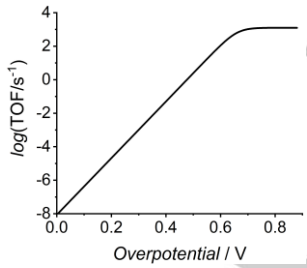

Figure 5. Catalytic Tafel plot for the reduction of CO_2 to CO by Fe(L)Cl in acetonitrile, in the presence of 0.6 M phenol (k_{cat} = 1250 s^{-1}, Table 1). E^0, the potential of the Fe^{II}/Fe^{I} couple in the absence of CO_2 and phenol, is set to – 2.00 V vs Fc^+/Fc (see Figure 1).

The Iron salophen is catalysing CO_2 electrochemical reduction at relatively low overpotential (in the range of several literature benchmarks based also on noble second and third row transition metals, see Table S1 in Supporting Information). The catalytic rate k_{cat} (or turnover frequency, *TOF*) is high (see the Catalytic Tafel plot for representative catalysts in Figure S1), although it is one order of magnitude lower with respect to the one observed for the iron tetraphenyl porphyrin (k_{cat} up to 10^4 s^{-1}),[14,33] the forerunner of this class of CO_2 reduction catalysts. The impressive improvement of catalytic performance for iron porphyrins in the latest years[34,35] suggests a large margin of catalyst optimization also for Fe–salophen catalyst. With this regard, a tetracationic iron porphyrin[35] stands as a clear outstanding performance catalyst with respect to the average, both in terms of low overpotential and of high k_{cat}; this win–win condition was ascribed to a favourable supramolecular interaction of the catalyst with carbon dioxide: a similar approach can thus be envisaged for iron salophen species, by proper functionalization of the ligand scaffold.[71,72] A primary task will be first to stabilize the catalyst towards the observed electrodeposition of heterogeneous Iron based materials. In this regard, reductive activation of the Fe(qpy) catalyst through a photochemical cycle has shown to improve the catalyst durability with respect to the electrochemical conditions;[38] the utilization of the title Fe(L) catalysts in light activated cycles is currently on going and will be reported in due course.

Conclusions

We have reported Iron complexes with an N_2O_2 type salophen ligand as a new class of molecular catalysts for the electrochemical reduction of CO_2. The main results can be summarized as follows: (i) the Fe-salophen species operate through an homogeneous pathway performing CO_2 to CO reduction in acetonitrile with phenol as the proton donor and with k_{cat} up to 10^3 s^{-1} at an overpotential of 0.65 V. (ii) The mechanism involves an electrogenerated mononuclear Fe^{I} intermediate, capable of binding of CO_2 and assisting C–O bond breaking of carbon dioxide with the formation of an Iron–carbonyl species. (iii) Under operating conditions, competitive electrodeposition of Fe nanoparticles occurs, which are active towards the hydrogen evolution reaction, with a minor formation of methane (ca 1 ÷ 2 % Faradaic efficiency). These results pave the way to the design and development of novel catalysts for sustainable and mechanistically oriented CO_2 reduction, exploiting Iron as a most abundant and cheap metal combined with a synthetically easy and scalable organic ligand. In this regard, the straightforward synthesis of functionalized salophen ligands can allow the preparation of a library of catalysts, that can be exploited for structure–reactivity correlations. An important perspective towards sustainability is related to the employement of the catalyst in gas phase or aqueous electrolyte based flow cells, exploiting its heterogeneization onto conductive supports. One possible drawback is the competitive evolution of hydrogen. In the present case, the stability of the catalyst in aqueous environment under the catalytic conditions should be also considered.

Experimental Section

See the Supporting Information for full experimental details on synthetic and characterization procedures, and of spectroscopic and electrochemical experiments.

Abbreviations

L = salophen ligand; TON = turnover number, TOF = turnover frequency; FOWA: foot–of–the–wave–analysis; Fc^+/Fc = ferrocenium/ferrocene couple; PhOH = phenol; HAc = acetic acid.

Acknowledgements

A.S. gratefully acknowledges financial support from Fondazione Cariparo (Project "SYNERGY", Progetti di Eccellenza 2018) and from the Department of Chemical Sciences at University of Padova (Project PHOETRY, P–DiSC #10BIRD2018–UNIPD). Partial financial support to M.R. from the *Institut Universitaire de France* (IUF) is gratefully thanked. M.B. acknowledges the Italian MIUR for the PRIN project Nanoredox (Prot. 2017PBXPN4). R.A. acknowledges the Erasmus internship program of the University of Padova for funding his research period at the Laboratoire d'Electrochimie Moléculaire, Université de Paris. Mauro Meneghetti, Stefano Mercanzin, Gianni Marin and Roberto Inilli, technicians at the department of chemical sciences, University of Padova, are acknowledged for their indispensable help in the set–up of all the experimental equipments.

Keywords: CO_2 reduction • Iron complex • Schiff base • Molecular electrocatalysis • Catalytic mechanism.

References

[1] W. Zhang, W. Lai, R. Cao, *Chem. Rev.* **2017**, *117*, 3717–3797.

[2] F. Möller, S. Piontek, R. G. Miller, U. P. Apfel, *Chem. - A Eur. J.* **2018**, *24*, 1471–1493.

[3] J.-M. Savéant, *Chem. Rev.* **2008**, *108*, 2348–2378.

[4] K. Li, X. An, K. Hyeon, M. Khraisheh, J. Tang, *Catal. Today* **2014**, *224*, 3–12.

[5] Q. Liu, L. Wu, R. Jackstell, M. Beller, *Nat. Commun.* **2015**, *6*, 1–15.

[6] Y. Yamazaki, H. Takeda, O. Ishitani, *J. Photochem. Photobiol. C Photochem. Rev.* **2015**, *25*, 106–137.

[7] R. Francke, B. Schille, M. Roemelt, *Chem. Rev.* **2018**, *118*, 4631–4701.

[8] X. M. Hu, S. U. Pedersen, K. Daasbjerg, *Curr. Opin. Electrochem.* **2019**, *15*, 148–154.

[9] J. J. Shi, X. M. Hu, M. R. Madsen, P. Lamagni, E. T. Bjerglund, S. U. Pedersen, T. Skrydstrup, K. Daasbjerg, *ACS Appl. Nano Mater.* **2018**, *1*, 3608–3615.

[10] X. M. Hu, H. H. Hval, E. T. Bjerglund, K. J. Dalgaard, M. R. Madsen, M. M. Pohl, E. Welter, P. Lamagni, K. B. Buhl, M. Bremholm, M. Beller, S. U. Pedersen, T. Skrydstrup, K. Daasbjerg, *ACS Catal.* **2018**, *8*, 6255–6264.

[11] A. Bagger, W. Ju, A. S. Varela, P. Strasser, J. Rossmeisl, *ChemPhysChem* **2017**, *18*, 3266–3273.

[12] L. Zhang, Z.-J. Zhao, J. Gong, *Angew. Chemie* **2017**, *129*, 11482–11511; *Angew. Chemie Int. Ed.* **2017**, *56*, 11326–11353.

[13] R. Kortlever, J. Shen, K. J. P. Schouten, F. Calle-Vallejo, M. T. M. Koper, *J. Phys. Chem. Lett.* **2015**, *6*, 4073–4082.

[14] H. Takeda, C. Cometto, O. Ishitani, M. Robert, *ACS Catal.* **2017**, *7*, 70–88.

[15] K. E. Dalle, J. Warnan, J. J. Leung, B. Reuillard, I. S. Karmel, E. Reisner, *Chem. Rev.* **2019**, *119*, 2752–2875.

[16] C. Costentin, M. Robert, J.-M. Savéant, *Chem. Soc. Rev.* **2013**, *42*, 2423–2436.

[17] S. Sato, T. Morikawa, T. Kajino, O. Ishitani, *Angew. Chemie* **2013**, *125*, 1022-1026; *Angew. Chemie, Int. Ed.* **2013**, *52*, 988–992.

[18] A. Genoni, D. N. Chirdon, M. Boniolo, A. Sartorel, S. Bernhard, M. Bonchio, *ACS Catal.* **2017**, *7*, 154–160.

[19] A. Dubey, L. Nencini, R. R. Fayzullin, C. Nervi, J. R. Khusnutdinova, *ACS Catal.* **2017**, *7*, 3864–3868.

[20] L. Rotundo, J. Filippi, R. Gobetto, H. A. Miller, R. Rocca, C. Nervi, F. Vizza, *Chem. Commun.* **2019**, *55*, 775–777.

[21] M. Bourrez, F. Molton, S. Chardon-Noblat, A. Deronzier, *Angew. Chemie* **2011**, *123*, 10077–10080; *Angew. Chemie, Int. Ed.* **2011**, *50*, 9903–9906.

[22] M. Wang, K. Torbensen, D. Salvatore, S. Ren, D. Joulié, F. Dumoulin, D. Mendoza, B. Lassalle-Kaiser, U. Işci, C. P. Berlinguette, M. Robert, *Nat. Commun.* **2019**, *10*, DOI 10.1038/s41467-019-11542-w.

[23] S. Ren, D. Joulié, D. Salvatore, K. Torbensen, M. Wang, M. Robert, C. P. Berlinguette, *Science (80-.).* **2019**, *365*, 367–369.

[24] V. Andrei, B. Reuillard, E. Reisner, *Nat. Mater.* **2020**, *19*, 189–194.

[25] R. Hedderich, *J. Bioenerg. Biomembr.* **2004**, *36*, 65–75.

[26] M. R. Dubois, D. L. Dubois, *Acc. Chem. Res.* **2009**, *42*, 1974–1982.

[27] J.-H. Jeoung, H. Dobbek, *Science (80-.).* **2007**, *318*, 1461 LP – 1464.

[28] A. Taheri, L. A. Berben, *Inorg. Chem.* **2016**, *55*, 378–385.

[29] M. Diego Rail, L. A. Berben, *J. Am. Chem. Soc.* **2011**, *133*, 18577–18579.

[30] N. D. Loewen, T. V. Neelakantan, L. A. Berben, *Acc. Chem. Res.* **2017**, *50*, 2362–2370.

[31] C. Costentin, S. Drouet, M. Robert, J. M. Savéant, *J. Am. Chem. Soc.* **2012**, *134*, 11235–11242.

[32] C. Costentin, M. Robert, J. M. Savéant, *Curr. Opin. Electrochem.* **2017**, *2*, 26–31.

[33] I. Bhugun, D. Lexa, J. M. Savéant, *J. Am. Chem. Soc.* **1996**, *118*, 1769–1776.

[34] C. Costentin, S. Drouet, M. Robert, J.-M. Savéant, *Science (80-.).* **2012**, *338*, 90 LP – 94.

[35] I. Azcarate, C. Costentin, M. Robert, J. M. Savéant, *J. Am. Chem. Soc.* **2016**, *138*, 16639–16644.

[36] L. Chen, Z. Guo, X. G. Wei, C. Gallenkamp, J. Bonin, E. Anxolabéhère-Mallart, K. C. Lau, T. C. Lau, M. Robert, *J. Am. Chem. Soc.* **2015**, *137*, 10918–10921.

[37] C. Cometto, R. Kuriki, L. Chen, K. Maeda, T. C. Lau, O. Ishitani, M. Robert, *J. Am. Chem. Soc.* **2018**, *140*, 7437–7440.

[38] C. Cometto, L. Chen, P. K. Lo, Z. Guo, K. C. Lau, E. Anxolabéhère-Mallart, C. Fave, T. C. Lau, M. Robert, *ACS Catal.* **2018**, *8*, 3411–3417.

[39] S. N. Pun, W. H. Chung, K. M. Lam, P. Guo, P. H. Chan, K. Y. Wong, C. M. Che, T. Y. Chen, S. M. Peng, *J. Chem. Soc. Dalt. Trans.* **2002**, 575–583.

[40] A. W. Nichols, S. Chatterjee, M. Sabat, C. W. MacHan, *Inorg. Chem.* **2018**, *57*, 2111–2121.

[41] P. Giorgio Cozzi, *Chem. Soc. Rev.* **2004**, *33*, 410–421.

[42] E. Pizzolato, M. Natali, B. Posocco, A. Montellano López, I. Bazzan, M. Di Valentin, P. Galloni, V. Conte, M. Bonchio, F. Scandola, A. Sartorel, *Chem. Commun.* **2013**, *49*, 9941–9943.

[43] A. M. López, M. Natali, E. Pizzolato, C. Chiorboli, M. Bonchio, A. Sartorel, F. Scandola, *Phys. Chem. Chem. Phys.* **2014**, *16*, 12000–12007.

[44] D. Toniolo, R. Scopelliti, I. Zivkovic, M. Mazzanti, *J. Am. Chem. Soc.* **2020**, *142*, 7301–7305.

[45] T. Ueda, N. Inazuma, D. Komatsu, H. Yasuzawa, A. Onda, S. X. Guo, A. M. Bond, *Dalt. Trans.* **2013**, *42*, 11146–11154.

[46] A. A. Isse, A. Gennaro, E. Vianello, C. Floriani, *J. Mol. Catal.* **1991**, *70*, 197–208.

[47] J. Shen, R. Kortlever, R. Kas, Y. Y. Birdja, O. Diaz-Morales, Y. Kwon, I. Ledezma-Yanez, K. J. P. Schouten, G. Mul, M. T. M. Koper, *Nat. Commun.* **2015**, *6*, 1–8.

[48] N. Sonoyama, M. Kirii, T. Sakata, *Electrochem. commun.* **1999**, *1*, 213–216.

[49] J. P. Costes, J. B. Tommasino, B. Carré, F. Soulet, P. L. Fabre, *Polyhedron* **1995**, *14*, 771–780.

[50] K. M. Kadish, G. Larson, D. Lexa, M. Momenteau, *J. Am. Chem. Soc.* **1975**, *97*, 282–288.

[51] A.B.P. Lever: Inorganic Electronic Spectroscopy, Elsevier, Amsterdam (1984).

[52] F. Lloret, J. Moratal, J. Faus, *J. Chem. Soc., Dalton Trans.*, **1983**, 1749–1753.

[53] M. Tagliapietra, A. Squarcina, N. Hickey, R. De Zorzi, S. Geremia, A. Sartorel, M. Bonchio, *ChemSusChem* **2017**, *10*, 4430–4435.

[54] D. M. Kurtz, *Chem. Rev.* **1990**, *90*, 585–606.

[55] K. J. Lee, N. Elgrishi, B. Kandemir, J. L. Dempsey, *Nat. Rev. Chem.* **2017**, *1*, DOI 10.1038/s41570-017-0039.

[56] C. W. Machan, M. D. Sampson, S. A. Chabolla, T. Dang, C. P. Kubiak, *Organometallics* **2014**, *33*, 4550–4559.

[57] A. Taheri, E. J. Thompson, J. C. Fettinger, L. A. Berben, *ACS Catal.* **2015**, *5*, 7140–7151.

[58] S. C. Cheng, C. A. Blaine, M. G. Hill, K. R. Mann, *Inorg. Chem.* **1996**, *35*, 7704–7708.

[59] C. Citek, P. H. Oyala, J. C. Peters, *J. Am. Chem. Soc.* **2019**, 141, 15211–15221.

[60] A. Zoleo, M. Brustolon, A. Barbon, A. Silvestri, G. Molin, S. Tonietto J. Cult. Heritage **2015**, *16*, 322–328.

[61] R. Cammack, C. E. Cooper, *Methods in Enzymology* **1993**, *227*, 353–384.

[62] I. Azcarate, C. Costentin, M. Robert, J. M. Savéant, *J. Am. Chem. Soc.* **2016**, *138*, 16639–16644.

[63] C. Costentin, M. Robert, J. M. Savéant, *Acc. Chem. Res.* **2015**, *48*, 2996–3006.

[64] A. W. Addison, L. K. M. Lau, M. Carpenter, M. Wicholas, *Inorg. Chem.* **1978**, *17*, 1545–1552.

[65] H. Y. V. Ching, X. Wang, M. He, N. Perujo Holland, R. Guillot, C. Slim, S. Griveau, H. C. Bertrand, C. Policar, F. Bedioui, M. Fontecave, *Inorg. Chem.* **2017**, *56*, 2966–2976.

[66] K. J. Lee, B. D. McCarthy, J. L. Dempsey, *Chem. Soc. Rev.* **2019**, *48*, 2927–2945.

[67] C. Cometto, L. Chen, D. Mendoza, B. Lassalle-Kaiser, T. C. Lau, M. Robert, *ChemSusChem* **2019**, *12*, 4500–4505.

[68] C. G. Margarit, N. G. Asimow, C. Costentin, D. G. Nocera, *ACS Energy Lett.* **2020**, *5*, 72–78.

[69] K. M. Waldie, A. L. Ostericher, M. H. Reineke, A. F. Sasayama, C. P. Kubiak, *ACS Catal.* **2018**, *8*, 1313–1324.

[70] V. V. Pavlishchuk, A. W. Addison, *Inorganica Chim. Acta* **2000**, *298*, 97–102.

[71] A. W. Nichols, C. W. Machan, *Front. Chem.* **2019**, *7*, 1–19.

[72] P. Gotico, B. Boitrel, R. Guillot, M. Sircoglou, A. Quaranta, Z. Halime, W. Leibl, A. Aukauloo, *Angew. Chemie* **2019**, *131*, 4552–4557; *Angew. Chemie, Int. Ed.* **2019**, *58*, 4504–4509.

10.1002/cssc.202001143

WILEY-VCH

Entry for the Table of Contents

FULL PAPER

Iron salophen complexes catalyze the electrochemical reduction of CO_2 to CO in acetonitrile with phenol as the proton donor through a mononuclear Fe^{I} intermediate.

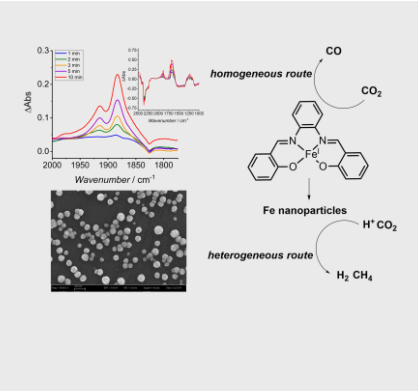

Ruggero Bonetto, Roberto Altieri, Mirko Tagliapietra, Antonio Barbon, Marcella Bonchio, Marc Robert and Andrea Sartorel**

Page No. – Page No.

Electrochemical conversion of CO_2 to CO by a competent Fe(I) intermediate bearing a Schiff base ligand